A Prescribed-Wake Vortex Line Method for Aerodynamic Analysis and Optimization of Multi-Rotor Wind Turbines

Aaron Rosenberg[1], Anupam Sharma[1,*]

Department of Aerospace Engineering,
Iowa State University, Ames, IA, 50011, USA

Abstract

This paper extends the prescribed wake vortex lattice/line method (VLM) to perform aerodynamic analysis and optimization of dual-rotor wind turbines (DRWTs). A DRWT turbine consists of a large, primary rotor placed co-axially behind a smaller, secondary rotor. The additional vortex system introduced by the secondary rotor of a DRWT is modeled while taking into account the singularities that occur when the trailing vortices from the secondary (upstream) rotor interact with the bound vortices of the main (downstream) rotor. Pseudo-steady assumption is invoked and averaging over multiple relative rotor positions is performed to account for the primary and secondary rotors operating at different rotational velocities. Our implementation of the VLM is first validated against experiments and blade element momentum theory results for a conventional, single rotor turbine. The solver is then verified against Reynolds Averaged Navier-Stokes (RANS) CFD results for two DRWTs. Parametric sweeps are performed using the proposed VLM algorithm to optimize a DRWT design. The problem with the algorithm at high loading conditions is highlighted and a solution is proposed that uses RANS CFD results to calibrate the VLM model.

*Corresponding author

Email addresses: aaronr@iastate.edu (Aaron Rosenberg), sharma@iastate.edu (Anupam Sharma)

1. Introduction

The dual-rotor wind turbine (DRWT) technology (see Fig. 1) has recently been investigated [1, 2, 3, 4, 5] as a higher efficiency alternative to conventional, single-rotor wind turbines (SRWTs). The technology uses two coaxial rotors to harness energy from wind. The two rotors can have different or same diameters, and can rotate with the same rotational speed (e.g., if they are on the same shaft) or independent of each other. DRWTs have additional parameters compared to SRWTs such as relative rotor sizes, rotation speeds, axial separation, etc. These parameters must be carefully chosen to optimize the aerodynamic performance of the DRWT. Due to the large parametric space that needs to be explored for such optimization, it is desirable to have an analysis method that is computationally inexpensive and can provide quick results.

Blade element momentum (BEM) theory based methods and vortex line/lattice methods have been used extensively in design and analysis of SRWTs. No straightforward extensions of these methods exist that enable a general analysis of multi-rotor wind turbines. In this paper, we present a methodology to extend the vortex line method to carry out aerodynamic analysis and optimization of DRWTs.

2. Vortex Line Method

The vortex line method is based on Prandtl's lifting line theory, which utilizes the laws of kinematics (Helmholtz vortex theorems) and dynamics (Kelvin's circulation theorem) of vortex lines. Potential flow is assumed and rotor blades are replaced by blade-bound vorticity (lifting lines). The bound vorticity for a blade section (airfoil) can be concentrated at a point or distributed along the airfoil chord/camber line; vorticity and circulation are related by Stokes' theorem. Helmholtz vortex theorems necessitate the existence of a single free-trailing vortex sheet per blade. They also define the distribution of the trailing vorticity; the strength of each trailing vortex is equal to the change in circulation along the lifting line.

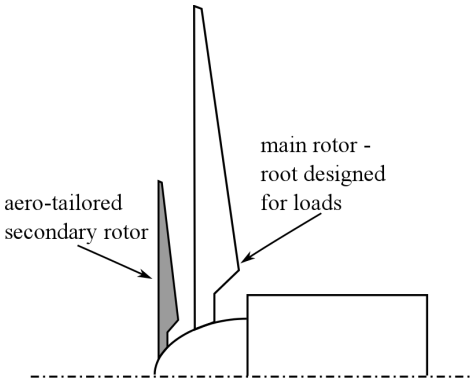

Figure 1: A schematic of the DRWT technology by Rosenberg *et al.* [1]

Velocity "induced" by vorticity is described by the Biot-Savart law. In an aircraft, the velocity induced on the wing by the trailing vortex sheet is referred to as "downwash". This downwash is responsible for induced drag in finite-span wings. The same concept can be applied to wind turbine rotor blades (or propeller blades), where the trailing vortex sheet becomes helical due to blade rotation. Induction determines the local flow velocity and, given blade geometry and operation specifications, the local blade-relative flow velocity and angle of attack. With prior knowledge of sectional lift and drag polars ($C_l-\alpha$ and $C_d-\alpha$ curves), the local lift and drag can be computed. Finally, the Kutta-Jukowski theorem links sectional lift to circulation around a blade section. Using these theorems, an iterative procedure can be obtained to compute spanwise distribution of circulation (or blade-bound vorticity) on turbine rotor blades (see e.g. Refs. [6, 7]).

Based on the treatment of trailing vorticity, the vortex line method can be classified as either *free wake* or *prescribed (fixed) wake* [8]. In the free-wake approach, mutual induction between trailing vortex elements is permitted and hence the wake evolves with time; the wake structure can deform substantially over time. In the prescribed-wake approach, mutual induction is ignored and the prescribed trailing vortex structure stays intact. Subtle changes to the wake structure that do not change the wake helix topology, such as helix pitch, tip radius etc. are permitted in the prescribed-wake approach until convergence is reached. These changes are specified as functions of some overall integrated quantity such as rotor thrust- or power coefficient. Figure 2 shows two views of the prescribed trailing vortex structure behind a 3-bladed wind turbine.

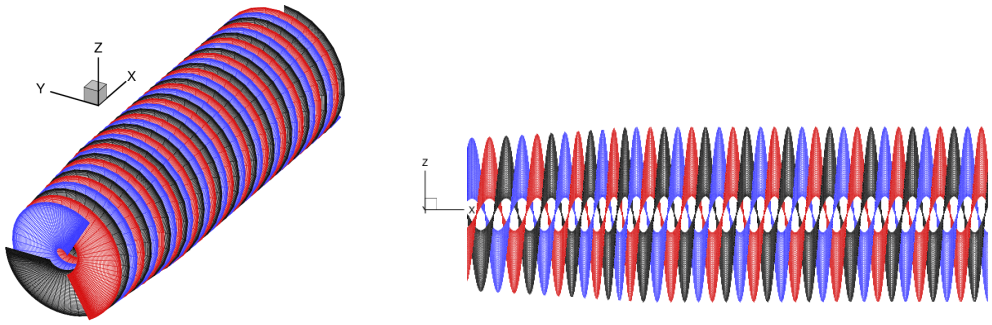

(a) Isometric view (b) Side view

Figure 2: Trailing wake vorticity behind a 3-bladed HAWT. The trailing vortex sheets of the three blades of the turbine are displayed with three different colors.

While the free-wake approach is of higher fidelity, it is computationally expensive [8] and can suffer from robustness issues. The prescribed-wake approach, on the other hand, is relatively quick and robust, but can be inaccurate if the fixed wake structure is poorly specified. We choose the prescribed-wake approach here as the objective is to explore a large design space during preliminary design and optimization of DRWTs. For our purpose, efficiency and robustness are more important than fidelity.

The particular implementation presented in Refs. [7, 9, 10] is adopted in our prescribed-wake vortex line method solver. Chattot [10] assumes 'wake equilibrium' to relate computed turbine power coefficient, C_P with that given by the 1-D momentum theory to obtain axial induction factor, a using the relation $C_P = 4a(1-a)^2$. This axial induction factor is then used to update the pitch of the trailing vortex helix in an iterative procedure until convergence is achieved. The problem with this approach is that axial induction is a multi-valued function of C_P (see Fig. 3). Typically, the solution corresponding to smaller axial induction factor is selected to set the helix pitch. While this strategy works for low-loading conditions, it is evident from Fig. 3 that this approach is incorrect for cases with high rotor disk loading. An alternative is to choose turbine thrust force coefficient, C_T to calculate a. However, if the 1-D momentum theory formula for C_T is chosen (i.e., $C_T = 4a(1-a)$), then the non-uniqueness problem still persists (see Fig. 3) although the range of operation is increased. We get around this non-uniqueness problem by using the empirical formula for C_T by Buhl [11] which incorporates corrections for high disk (rotor) loading. The formula (Eq. 1, with $F = 0.9$) provides a one-to-one mapping between a and C_T.

$$C_T(a) = \begin{cases} 4aF(1-a) & \text{if } 0 \leq a \leq 0.4 \\ \dfrac{8}{9} + \left(4F - \dfrac{40}{9}\right) a + \left(\dfrac{50}{9} - 4F\right) a^2 & \text{if } 0.4 < a \leq 1 \end{cases} \tag{1}$$

The VLM solver algorithm used for this study is presented as a flowchart in Fig. 4. In the later sections we present that even after using Eq. 1, the VLM solver gives unacceptable results for DRWTs at high disk loading conditions. An alternative strategy to mitigate this problem is described in Sec. 4.

2.1. Validation

Our implementation of the vortex line method is validated against experimental data and blade element momentum (BEM) theory predictions. The

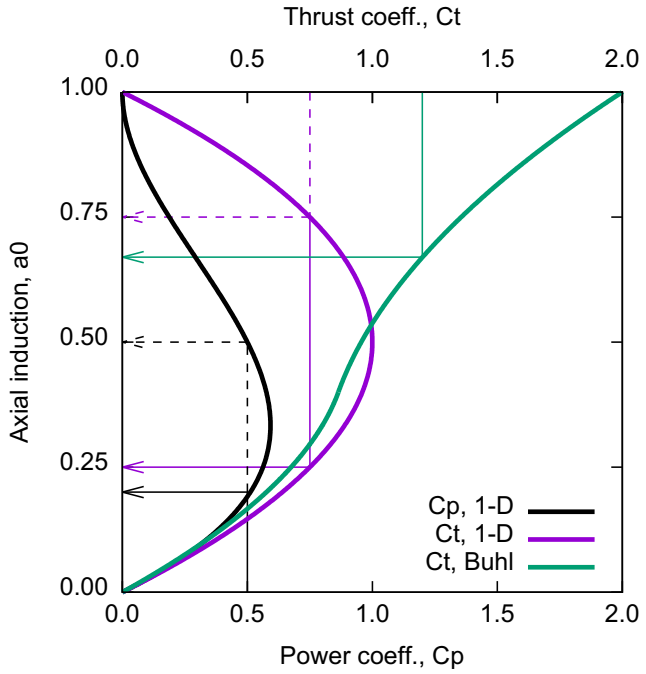

Figure 3: Functions to obtain axial induction factor, a from C_P and C_T given by 1-D momentum theory, and from C_T given by Eq. 1.

three-bladed, stall controlled, 95 kW Tellus T-1995 is used for validation. The turbine rotor diameter is 19 m. The turbine rotor blade chord and twist distributions are plotted in Fig. 5.

Figure 6 compares turbine characteristic curves as predicted by the prescribed wake vortex line method solver against measured data as well as BEM predictions. Variations of power coefficient, C_P and thrust force coefficient, C_T with tip speed ratio, λ are reasonably well predicted by the vortex line method solver. Code-to-code comparisons (between vortex line method and BEM) of span-wise variations of torque force coefficient, $c_{\tau F}$ and thrust force coefficient, c_T are presented at the tip speed ratio, $\lambda = 7.0$ in Fig. 7. The agreement between the two methods is very good. This verifies the solver capability for single rotor wind turbines. In the following section we present our approach to extend the vortex line method to DRWTs.

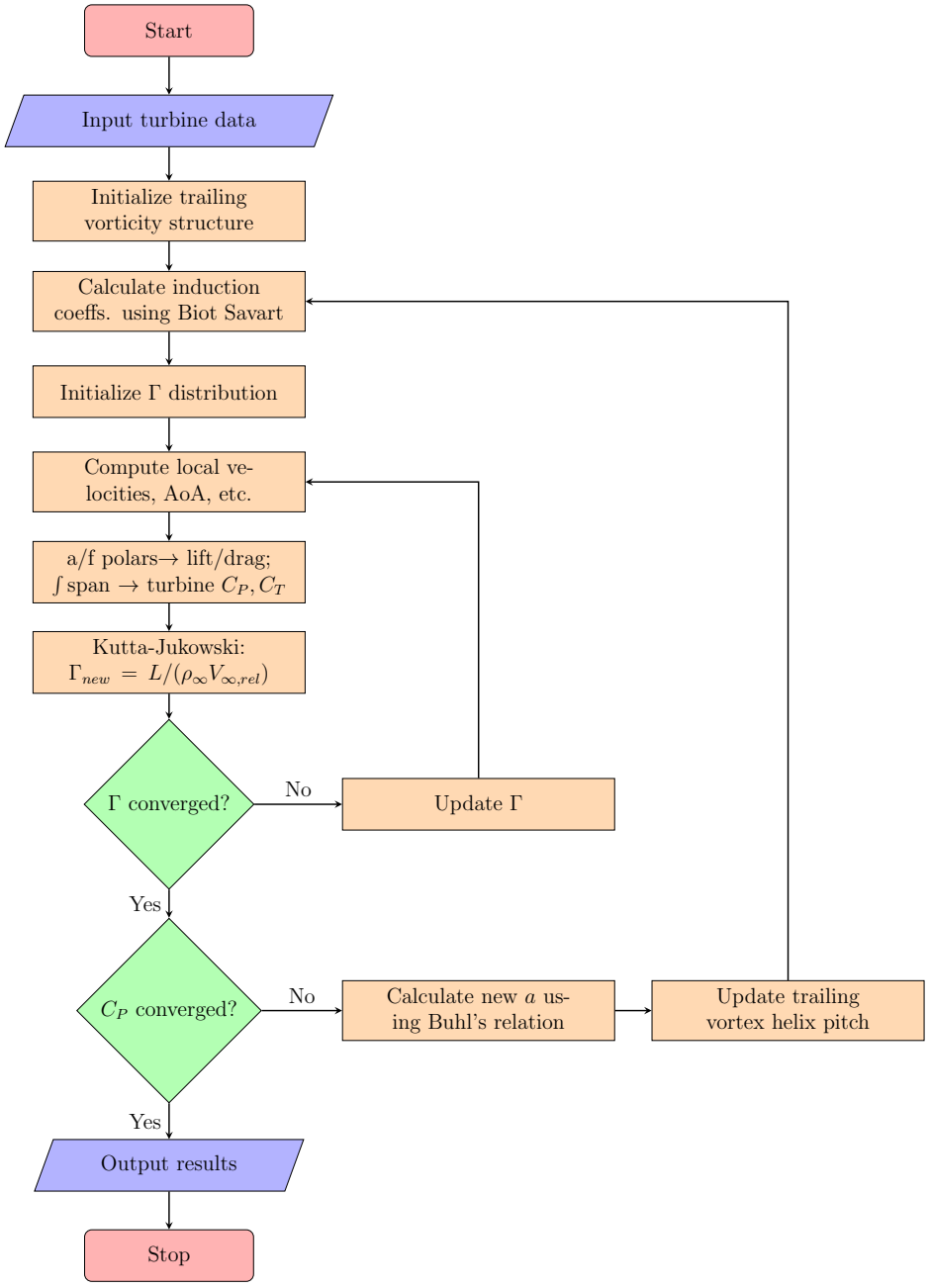

Figure 4: Prescribed-wake vortex line method algorithm for analysis of single-rotor wind turbine aerodynamics

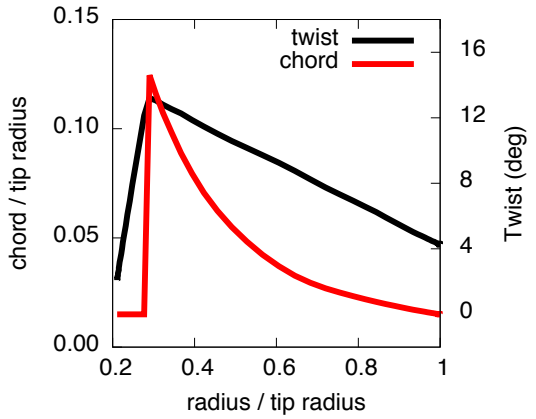

Figure 5: Non-dimensional chord and twist distributions for the model Tellus T-1995 turbine used for validation.

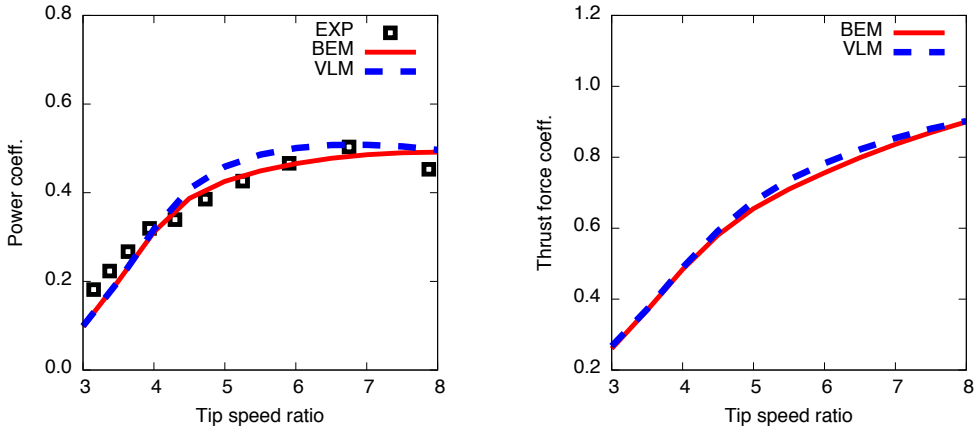

(a) $C_P - \lambda$ (b) $C_T - \lambda$

Figure 6: Comparisons with experimental data and against BEM results for the Tellus T-1995 turbine

3. Extension to Dual-Rotor Wind Turbines

Several aspects need to be considered when evaluating aerodynamic performance of dual-rotor wind turbines using a vortex line method:

1. Both rotors have trailing vortex sheets; this has to be accounted for when calculating induction using the Biot-Savart law. Also bound vorticity on the rotors mutually influence the induction on each other.

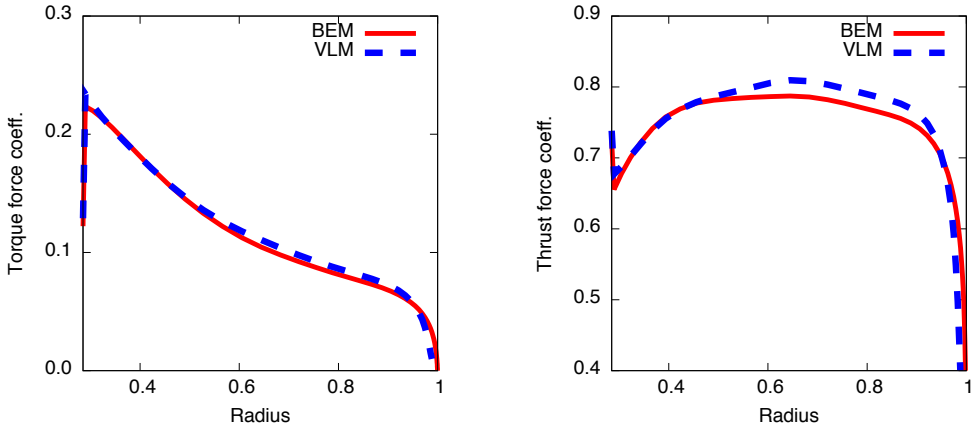

(a) c_{τ_F} (b) c_T

Figure 7: Comparisons of radial variation of force coefficients at $\lambda = 7.0$ against BEM results for the Tellus T-1995 turbine

2. If the two rotors rotate independently, then the problem becomes inherently unsteady; approximations need to be made to solve it as a steady problem.
3. If the two rotors are very close, potential flow effects (due to finite blade thickness) also come into play.

To account for mutual induction between the bound and trailing vortices of the two rotors of a DRWT, we first need to setup the associated vortex lines/lattices. Figure 8 shows the vortex lattice structure of a DRWT. Two sets of helices are now present; one set each for the two rotors. The pitch of the two helices is set to be the same since the trailing vorticity is convected by the same flow speed. Equation 1 is used to determine the area-average induction, a, which then determines the pitch of the helices. For DRWTs, an equivalent area-weighted $C_{T,eq}$ is used with Eq. 1, where

$$C_{T,eq} = C_{T,m} + \frac{A_s}{A_m} C_{T,s}, \tag{2}$$

and subscripts 'm' and 's' refer to the main rotor and the secondary rotor respectively; 'A' is area of rotor disk. Once the vorticity structure is set, computation of induction coefficients using the Biot-Savart law is straightforward. It should be emphasized again that induction from bound vorticity

of both rotors has to computed and added to the induction computed using trailing vorticity. Another complexity can arise in computing induction. A

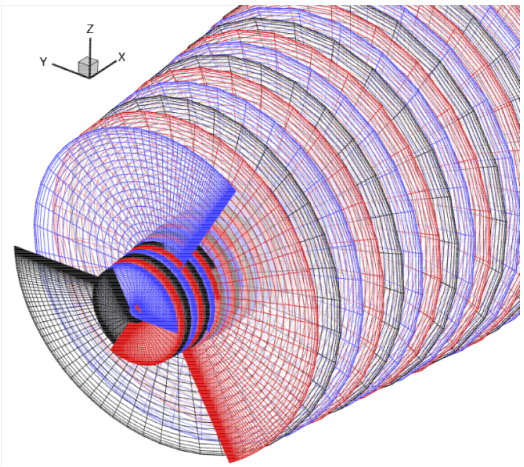

Figure 8: Trailing wake vorticity behind the two rotors of a dual-rotor wind turbine. Each rotor is three bladed. The three colors: red, blue, and black denote the trailing vorticity from each blade of the two rotors.

singularity arises if any point on the trailing vortex structure of the upstream rotor coincides with a point on a blade of the downstream rotor where induction is computed. This singularity is averted by imposing a minimum threshold on the distance between two such points - essentially to avoid division by zero in Biot-Savart law.

If the two rotors of a DRWT rotate independently, the problem becomes unsteady even if uniform inflow is assumed. This is because of the relative rotation of the two rotors and the time-varying change in lift as a result. Unsteady computations, even with a vortex line method are expensive and not very suitable for optimization purposes. We therefore use a pseudo-steady approximation, wherein we compute turbine performance for different relative angular positions of the two rotors. Averaging over such steady solutions gives the net performance of a DRWT. Figure 9 plots the variation in $\%C_P$ of a DRWT for twelve relative rotor positions. The pattern repeats after 120^0 due to periodicity in the problem (both rotors are three bladed). The maximum variation is observed to be less that 0.5%. For production runs, averaging is performed over five angular positions.

In the present approach, we neglect thickness effects by assuming that axial separation between the rotors is greater than the rotor blade chord.

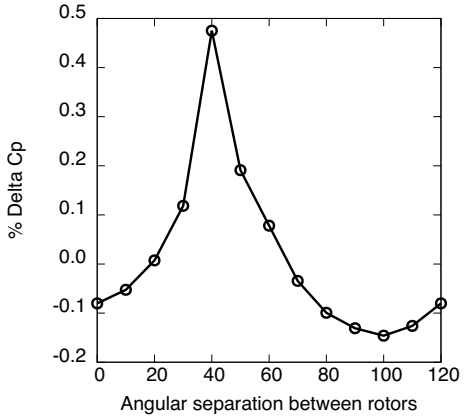

Figure 9: Predicted variation in % C_P of a DRWT with relative angular position between the primary and the secondary rotors.

Rosenberg et al. [1] suggest that the optimum axial separation for enhanced isolated rotor aerodynamic performance is about 0.2 × main rotor diameter, which is much greater than the maximum blade chord of the main rotor. Thus, the approximation to neglect potential effects due to blade thickness should be valid for such turbines.

3.1. Verification with CFD

The proposed extended vortex line method to analyze dual-rotor wind turbines is verified against results obtained using the Reynolds Averaged Navier-Stokes + actuator disk (RANS/AD) method described in Rosenberg et al. [1] and Selvaraj [12]. Subtle aspects of this RANS/AD methodology are summarized here for completeness.

3.1.1. RANS/AD Method

The RANS/AD method [1, 12] solves the incompressible RANS equations (Eq. 3) with the rotor blades modeled as body forces (actuator disk). The governing equations are

$$\begin{aligned} \frac{\partial \bar{u}_i}{\partial x_i} &= 0, \text{ and,} \\ \bar{u}_j \frac{\partial \bar{u}_i}{\partial x_j} &= -\frac{1}{\rho}\frac{\partial \bar{p}}{\partial x_i} + \nu \frac{\partial^2 \bar{u}_i}{\partial {x_j}^2} - \frac{\partial \overline{u_i' u_j'}}{\partial x_j} + \frac{f_i}{\rho}. \end{aligned} \tag{3}$$

In the above, the overbar denotes time averaging. The Reynolds stress tensor, $\overline{u_i' u_j'}$ is modeled using the standard two equation, $k-\epsilon$ turbulence model[13]. The term f_i represents the body force per unit volume and is computed using user-prescribed airfoil polars and local flow velocity. The body force, f_i is spatially distributed - the distribution takes a Gaussian shape along the flow direction and uniform along the radial direction. Linear interpolation is used to compute f_i at computational grid points. Axisymmetric flow assumption is made to reduce the problem to two dimensions.

This RANS/AD model is implemented in OpenFOAM and has been validated against experimental data as well as Blade Element Momentum (BEM) theory solutions for single-rotor turbines [1, 12, 14]. Recently, we have improved this methodology by incorporating Prandtl's tip loss correction following Mikkelsen [15]. The RANS/AD results presented in this paper use this improved model and are therefore slightly different from those in Refs. [12, 14].

The use of the RANS/AD CFD method to analyze DRWTs is described in Rosenberg et al. [1]. Figure 10 shows an example computational grid and CFD solution for flow over a DRWT. In this example the secondary rotor tip radius is 0.4 times that of the main rotor, and the main and secondary rotors are placed at $x = +0.1$ and $x = -0.1$ respectively.

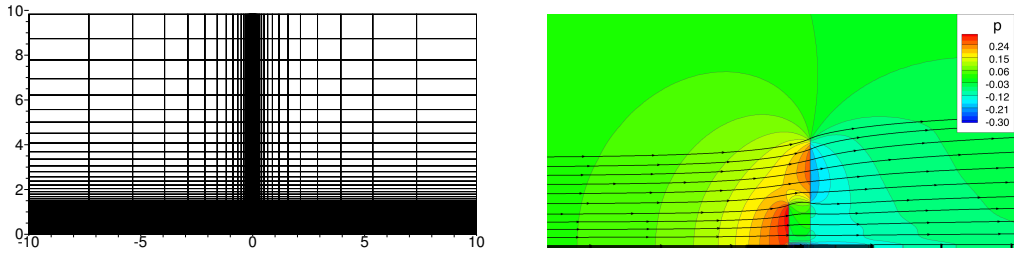

(a) Grid (b) Solution (zoom view)

Figure 10: Numerical setup and result of the RANS/AD method applied to a DRWT: (a) axisymmetric grid (every fifth point shown for clarity), and (b) pressure contours and streamlines (zoomed in near the DRWT).

Two DRWT configurations are chosen for code-to-code comparisons between the proposed VLM and RANS/AD methods. The radius of the secondary rotor is selected to be 25% and 40% of the main rotor radius for the two designs. However, both the DRWT configurations use the same *non-dimensional* rotors for the main rotor as well as the secondary rotor.

Figures 11 and 12 compare span-wise variation of local angle of attack and torque force coefficients. Good agreement between VLM and RANS/AD results is observed for both primary and secondary rotors for the two DRWTs. The differences are largest at the radial location corresponding to the tip radius of the secondary rotor. This is expected for two reasons: (1) the turbulence in the RANS/AD simulations will diffuse the trailing vortex sheet of the secondary rotor while the VLM has no such mechanism, and (2) the AD model smears the effect of individual blade over the entire disk, whereas the VLM models each individual blade trailing vorticity independently. Even though VLM results are averaged from multiple relative angular positions of the two rotors in the proposed algorithm, it should be realized that this averaging is not the same as azimuthally averaging the trailing vortices, which is what happens in the RANS/AD method.

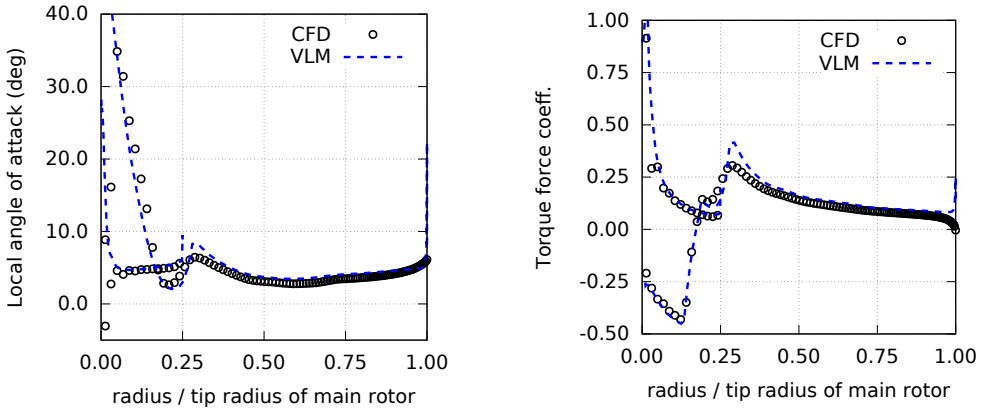

(a) Angle of attack

(b) Torque force coeff.

Figure 11: Comparisons between CFD and VLM of spanwise variations of angle of attack and torque force coefficient for the following parameters of the secondary rotor: $r/r_{tip} = 0.25$ and $\lambda = 8.0$.

4. Optimization of a Dual-Rotor Wind Turbine

The validated vortex line method is used to perform parametric sweeps for optimizing a DRWT design. One such study was presented by Rosenberg et al. [1] where the secondary rotor diameter, tip speed ratio, and rotor-rotor separation were varied and an optimal configuration obtained. In this

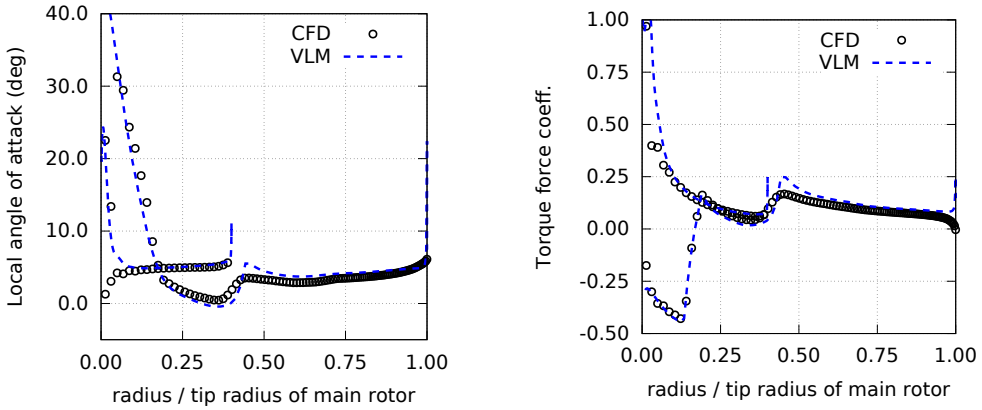

(a) Angle of attack

(b) Torque force coeff.

Figure 12: Comparisons between CFD and VLM of spanwise variations of angle of attack and torque force coefficient for the following parameters of the secondary rotor: $r/r_{tip} = 0.40$ and $\lambda = 8.0$.

paper, we focus on varying only two parameters: rotor-rotor separation and secondary rotor tip speed ratio.

Figure 13 compares the results of parametric sweeps performed using the RANS/AD method and the vortex line method described in the previous sections. The failure of the VLM model is apparent at high loading conditions - in the top right corner in Fig. 13 (b). The model predicts very large and sudden variations in C_P for highly loaded DRWT designs, whereas RANS/AD results suggest uniformly reducing C_P in that region. In the following section, we investigate and draw inspiration from the RANS/AD results to improve the robustness and accuracy of the proposed multi-rotor VLM model for high loading conditions.

4.1. Enhancements to the VLM Model

Results from RANS/AD analysis of the Tellus T-1995 95 kW wind turbine are used to calibrate the prescribed wake vortex line method algorithm. In particular, the distribution of trailing vorticity is adapted based on CFD results as described below.

Chattot's algorithm [10] assumes that the axial induction increases linearly from its initial value, a_0, directly behind the rotor to $2a_0$ at the Trefftz plane. The Trefftz plane is assumed to be located at x_{r3}, which denotes the

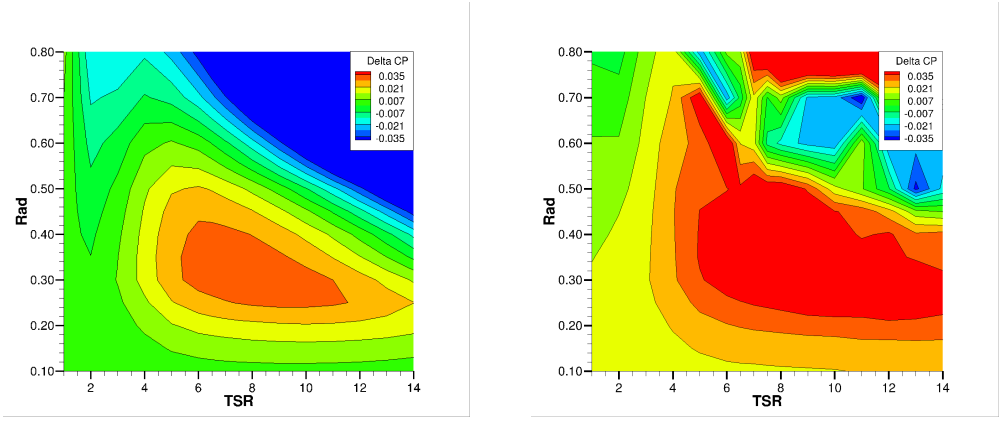

(a) RANS (b) VLM

Figure 13: Parametric sweep varying the secondary rotor tip speed ratio and tip radius. Contours of difference in aerodynamic power coefficient, $\Delta C_P = C_{P\text{DRWT}} - C_{P\text{SRWT}}$ as predicted by (a) RANS and (b) VLM are shown.

distance the trailing vortex helix convects downstream while the rotor completes three revolutions. x_{r3} is related to the turbine geometry and operating conditions as

$$x_{r3} = 3 \times 2\pi R(1 - a_0)/\lambda. \tag{4}$$

Figure 14 plots the RANS/AD predicted normalized axial induction (a/a_0) with normalized downstream axial distance (x/x_{r3}). As apparent in Fig. 14, neither does the axial induction reach (even asymptotically) the value of $2a_0$, nor is the variation with downstream distance linear. Only under very low loading conditions does the axial induction at x_{r3} begin to approach $2a_0$; for such conditions the variation with axial distance is highly nonlinear. This is largely because the turbulence model in the RANS/AD method diffuses the wake/vortex sheet. It should be noted that such diffusion is representative of what happens in the physical world.

We attempt to incorporate this in the VLM by empirically relating the axial induction at x_{r3} with the initial axial induction (Eq. 5) and fitting a hyperbolic tangent function (Eq. 6). The fitted curves are plotted in Fig. 15. The constant $B = 2$ is chosen such that the distribution closely matches the RANS data at the design tip-speed ratio ($\lambda = 7$) of the turbine. It should be emphasized that this model calibration is performed using RANS/AD results

of a *single-rotor* turbine.

$$a_{x_{r3}} = 0.47\, C_T + 0.03 \tag{5}$$

$$a(x) = a_0 \left(\left(\frac{a_{x_{r3}}}{a_0} - 1 \right) \frac{\tanh(B \times x/x_{r3})}{\tanh(B)} + 1 \right) \tag{6}$$

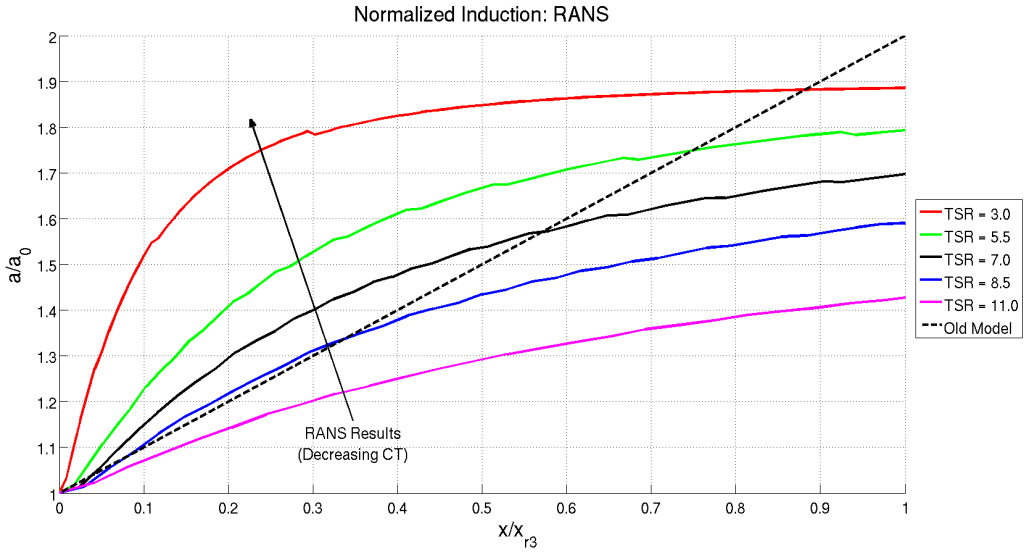

Figure 14: RANS results of downstream axial induction from the Tellus T-1995

The parametric sweeps are repeated with these modifications to the VLM algorithm. The results, plotted in Fig. 16, show that the predictions improve with the proposed modifications to the prescribed wake method. The proposed algorithm is more robust and the large variations in ΔC_P, as seen in Fig. 13 (b), are eliminated. A good qualitative agreement is observed between the RANS/AD predictions and the new VLM predictions of C_P enhancement with DRWTs. With this ability, the proposed prescribed wake vortex line method can be used to carry out preliminary design/analysis of dual-rotor wind turbines.

It should be noted that incorporating the modified wake distribution leads to an under-prediction of $C_{P_{max}}$ for the Tellus T-1995 turbine by roughly 7%. The reason for this has yet to be determined. However, for the purpose of determining an optimal dual-rotor configuration, the trend in ΔC_P is of

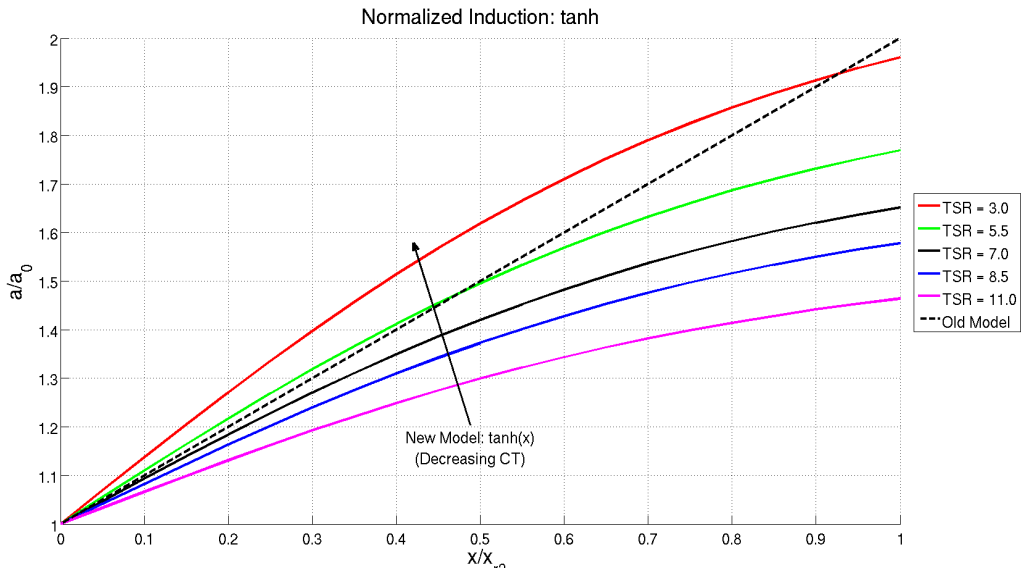

Figure 15: Empirical axial induction distribution inspired by RANS results

higher interest than absolute power output. Regardless, the cause for this disparity is being investigated.

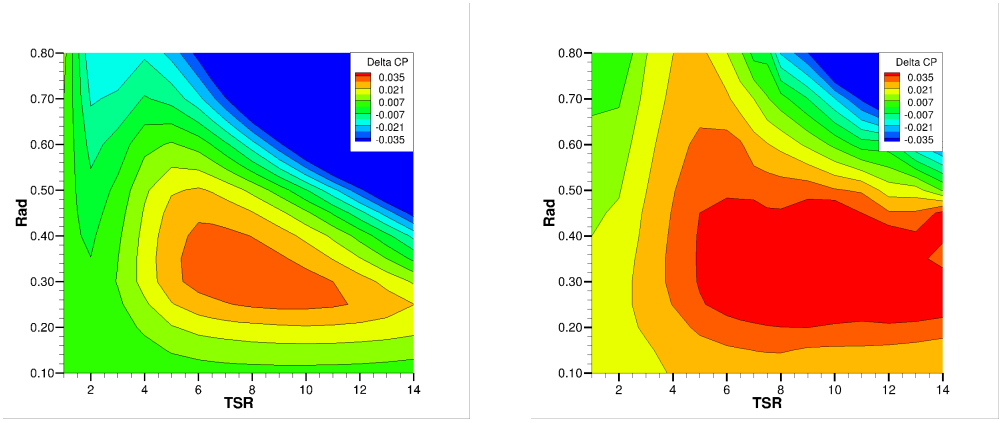

(a) RANS (b) VLM

Figure 16: Parametric sweep results with RANS/AD-guided calibration of the VLM. Contours of difference in aerodynamic power coefficient, $\Delta C_P = C_{P\mathrm{DRWT}} - C_{P\mathrm{SRWT}}$ as predicted by (a) RANS and (b) enhanced VLM are shown.

5. Conclusions

A prescribed wake vortex line method (VLM) to perform aerodynamic analysis and optimization of dual-rotor wind turbines is proposed. The method is first validated against experimental data and blade element momentum (BEM) theory results for a conventional, single-rotor wind turbine. The agreement between the measured and predicted power curves is reasonable. The agreement between VLM and BEM predictions is very good for torque force coefficient and acceptable for thrust force coefficient.

The method is extended to analyze dual-rotor wind turbines by assuming pseudo-steady flow and averaging results over multiple relative rotor phase angles. The trailing vortices of both rotors of the DRWT convect with the same flow velocity and hence the associated vortex helices are assumed to have the same pitch. Singularities in Biot-Savart's formula are avoided by enforcing a minimum threshold on spacing between the vortex element center and the point where induction is calculated. Comparisons made with RANS/AD CFD simulations (where the turbine rotors are modeled as actuator disks) show good agreement in predicted spanwise profiles of torque force coefficient and angle of attack.

Parametric sweeps, varying the secondary rotor radius and tip speed ratio are carried out using the proposed VLM method. Initial comparisons with default variable settings show that the method cannot handle high loading cases. The trailing vortex helix structure (particularly the axial pitch variation) is calibrated using RANS/AD CFD results. The calibration makes the VLM stable and the agreement between the VLM and RANS/AD optimization results is much improved.

6. Acknowledgment

Funding for this research was provided by the National Science Foundation National Science Foundation (Grant #NSF/CBET-1438099), the Iowa Energy Center (Grant #14-008-OG), and the Iowa Space Grants Consortium (Grant #475-20-5). Computational resources used for this research were provided by NSF XSEDE (Grant #TG-CTS130004).

References

[1] A. Rosenberg, S. Selvaraj, A. Sharma, A novel dual-rotor turbine for increased wind energy capture, Journal of Physics: Conference Series 524 (2014).

[2] B. Moghadassian, A. Rosenberg, H. Hu, A. Sharma, Numerical investigation of aerodynamic performance and loads of a novel dual rotor wind turbine, in: AIAA Science and Technology Forum and Exposition (SciTech2015).

[3] H. Hu, Z. Wang, A. Ozbay, W. Tian, A. Sharma, An experimental investigation on the wake characteristics behind a novel twin-rotor wind turbine, in: AIAA Science and Technology Forum and Exposition (SciTech2015).

[4] S. N. Jung, T. S. No, K. W. Ryu, Aerodynamic performance prediction of a 30kw counter-rotating wind turbine system, Renewable Energy 30 (2005) 631–644.

[5] A. Ozbay, W. Tian, H. Hu, An experimental investigation on the aeromechanics and near wake characteristics of dual-rotor wind turbines (drwts), in: AIAA Science and Technology Forum and Exposition (SciTech2014).

[6] D. Kocurek, Lifting surface performance analysis for horizontal wind axis turbines, Technical Report SERI/STR-217-3163; DE87001176, Solar Energy Research Institute, Computational Methodology Associates, 2900 Steve Drive, Hurst, Texas, USA, 1987.

[7] J.-J. Chattot, Design and analysis of wind turbines using helicoidal vortex model, Computational Fluid Dynamics Journal 11 (2002) 50–54.

[8] J. G. Leishman, Aerodynamics of horizontal axis wind turbines, in: Advances in Wind Energy Conversion Technology, Springer, 2011, pp. 1–69.

[9] J.-J. Chattot, Optimization of propellers using helicoidal vortex model, Computational Fluid Dynamics Journal 10 (2002) 429–438.

[10] J.-J. Chattot, Wind turbine aerodynamics: analysis and design, International Journal of Aerodynamics 1 (2011) 404–444.

[11] M. Buhl, A new empirical relationship between thrust coefficient and induction factor for the turbulent windmill state, 2005.

[12] S. Selvaraj, Numerical Investigation of Wind Turbine and Wind Farm Aerodynamics, Master's thesis, Iowa State University, 2014.

[13] B. Launder, B. Sharma, Application of the energy-dissipation model of turbulence to the calculation of flow near a spinning disc, Letters in heat and mass transfer 1 (1974) 131–137.

[14] S. Selvaraj, A. Chaves, E. Takle, A. Sharma, Numerical prediction of surface flow convergence phenomenon in windfarms, 2013.

[15] R. Mikkelsen, Actuator Disk Models Applied to Wind Turbines, Ph.D. thesis, Technical University of Denmark, 2003.